Harnessing Biomimetic Catch Bonds to Create Mechanically Robust Nanoparticle Networks

Balaji V. S. Iyer, Victor V. Yashin and Anna C. Balazs*

Chemical Engineering Department

University of Pittsburgh, Pittsburgh, PA 15261

*Corresponding author; e-mail address: balazs@pitt.edu

Abstract

Using computer simulations, we investigate the mechanical properties of a network of polymer-grafted nanoparticles (PGNs) that are interlinked by labile "catch" bonds. In contrast to conventional "slip" bonds, the life time of catch bonds can potentially increase with the application of force (i.e., the rate of rupture can decrease). In effect, the bond becomes stronger under an applied force (if the strain rate is sufficiently high). Subjecting the PGN networks to a tensile deformation, we find that the networks encompassing catch bonds exhibit greater ductility and toughness than the networks interconnected by slip bonds. Moreover, when the applied tensile force is released, the catch bond networks exhibit lower hysteresis and faster relaxation of residual strain than the slip bond networks. The effects of the catch bonds on the mechanical behavior are attributed to transitions between two conformational states, which differ in their sensitivity to force. The findings provide guidelines for creating nanocomposite networks that are highly resistant to mechanical deformation and show rapid strain recovery.

I. Introduction

One of the vital components in materials that can withstand significant strain without undergoing catastrophic failure is reactive, labile chemical bonds, which readily reform once they are broken [1,2]. This concept lies at the heart of such materials as dual cross-linked polymer-grafted nanoparticle (PGN) networks [3-7]. These materials encompass nanoparticles that are decorated with end-grafted polymers. The free ends of these polymers contain reactive groups that form bonds with reactive groups on neighboring chains. Some fraction of these bonds are labile connections and the other fraction are less reactive, higher strength "permanent" bonds, which do not reform after being broken. Due to the presence of both the labile and permanent bonds, the material is referred to as a "dual cross-linked" network. Using computational modeling, we showed that when this network is subjected to a tensile deformation, the labile bonds allow the nanoparticles to "reshuffle" by forming bonds with new neighbors as connections with previous partners are broken [7]. This reshuffling allowed the network to undergo a degree of self-healing even as the material was strained and in this manner, the dual cross-linked PGNs displayed remarkable ductility and strength. Hence, the presence of the labile bonds led to an improvement in the mechanical robustness of the material

In the previous studies [3-8], the labile bonds were modeled as traditional "slip" bonds [9], where the lifetime of the bond decreases with an applied tensile force. There is, however, a class of non-covalent chemical bonds, known as "catch" bonds [10-20], where the bond lifetime increases with force. On a conceptual level, catch bonds behave much as the finger trap toy; the harder you pull, the more tightly your fingers become bound by the encasing cylindrical tube [18]. Catch bonds play a crucial role in biological processes [11-20], especially in the binding of

leukocytes to the extracellular matrix [11-15]. Recently, there has been an effort to synthesize small molecules that exhibit catch bond behavior [21,22].

In the ensuing study, we examine the properties of PGN networks where the particles are interconnected by labile catch bonds, as shown in Fig. 1. Given that the catch bonds become stronger with an applied tensile force, we hypothesize that a PGN network involving these bonds will exhibit unprecedented resistance to deformation. We also anticipate that the catch bonds will enable the network to display significant self-healing behavior. To test these hypotheses, we undertake the simulations described below, where we adapt our previous model for the PGN networks [3-8] to include the catch bonds. Using this new model, we determine the response of the system to mechanical deformation and contrast the behavior of systems interconnected by slip bonds to those that are bound by the catch bonds. As we show below, the catch bonds do indeed provide new opportunities for creating composites with an exceptional response to applied tensile forces, including self-healing properties and low hysteresis as the material is repeatedly subjected to loading and unloading of the force.

We start by detailing our approach and relating our simulation parameters to physical experimental values. We then analyze the response of the system to varying levels of strain, as well as multiple cycles of mechanical deformation. We emphasize that to date such materials have not yet been synthesized, and hence, these predictions can prove useful in creating a new class of mechanically robust nanocomposites.

II. Methodology

The fundamental unit in our system consists of a spherical, rigid nanoparticle of radius r_0 that is decorated with end-grafted polymers, which form a corona around the particle. The corona chains are in the semi-dilute regime and assumed to be in a good solvent; the thickness of the

corona is given by $H = qr_0$. In the ensuing discussion, all the length scales in the system are given with respect to the core radius r_0 , and hence, we consider a polymer-grafted nanoparticle (PGN) of core radius unity and a corona thickness q .

The ends of the corona chains encompass reactive groups and the reactive groups on the neighboring PGNs interact to form either a strong ("permanent") or a labile bond (see Fig. 1). By means of these bonds, the PGNs are cross-linked into a swollen network. Both the permanent and labile bonds can rupture, but the only labile bonds can reform after they have ruptured.

In this coarse-grained approach, we model the interaction between two PGNs by a sum of interaction potentials: $U_{int} = U_{rep} + U_{coh} + U_{link}$. The term U_{rep} characterizes the repulsive interactions between the coated nanoparticles and is given by [23]:

$$\frac{U_{rep}(R)}{k_B T} = \frac{5}{18} f^{3/2} \times \begin{cases} -\ln(R/\sigma) + (1 + f^{1/2}/2)^{-1}, R \le \sigma \\ (1 + f^{1/2}/2)^{-1} (\sigma/R) \exp[-f^{1/2}(R-\sigma)/2\sigma], R > \sigma \end{cases} \quad (1)$$

Here, f is the number of arms, R is the center-to-center inter-particle separation and $\sigma = 2(1+q)(1+2f^{-1/2})^{-1}$ is the range of the potential [24,25]. The attractive cohesive interaction between the coated nanoparticles is described by a pseudopotential U_{coh}, which is constant for small values of R and balances the repulsion at the corona edges to allow for overlap between neighboring coronas. This potential is chosen to have the following form [26]:

$$U_{coh}(R) = -C\{1 + \exp[(R-A)/B]\}^{-1} \ , \quad (2)$$

where C is an energy scale, and A and B are length scales that determine the respective location and width of the attractive well in the potential.

The term U_{link} describes the attractive interaction between two particles linked by the bonded polymer arms. The attractive force acting between two bonded particles is given by [7]:

$$F_{link}(r) = N_b \kappa(r) r \, , \quad (3)$$

where N_b is the number of bonds formed between the given pair of particles, and $\kappa(r)$ is the spring stiffness, which increases progressively with the chain end-to-end distance $r = R - 2$. We use the following equation, obtained for a worm-like chain [27], to calculate $\kappa(r)$:

$$\kappa(r) = k_B T R_0^{-2} \{1 + 2[1 - r^2 (2L)^{-2}]^{-2}\} \ . \qquad (4)$$

Here, $2L$ is the contour length of the chain formed by bonding two polymer arms of length L, $R_0^2 = 4 l_p L$ is the mean-square end-to-end distance of the latter chain, and l_p is its persistence length. The value of N_b in eq. (3) depends on the extent of overlap between the coronas of the nanoparticles, and on the kinetics of bond formation and rupture [3,7].

Beyond specifying whether the bonds are permanent or labile, we also identify the labile bonds as being either "slip" or "catch" bonds. The permanent bonds, on the other hand, are assumed to behave as slip bonds. The key difference between the slip and the catch bonds lies in their response to an applied tensile force, and in particular, to the force-dependent rate of bond rupture [18-20] (see Fig. 2). Namely, the application of force accelerates the rupturing of the slip bonds. For catch bonds, however, the rate of rupture can both increase and decrease, depending on the force exerted on the bond (as discussed further below).

The effect of force on the rupture rate of the slip bonds can be described by the Bell model [9]. (In the ensuing discussion, the subscript p denotes a permanent bond and l indicates a labile bond.) According to the Bell model, the force exerted on the bond, F, acts to lower the energy barrier, $U_0^{(p,l)}$, separating the bound and free states, and leads to an exponential increase in the bond rupture rate, $k_r^{(p,l)} = k_{0r}^{(p,l)} \exp(\gamma_0 F)$, where $k_{0r}^{(p,l)} = \nu^{(p,l)} \exp(-U_0^{(p,l)} / k_B T)$ is the rupture rate in the absence of force [9,28-30]. (In the latter expression, $\nu^{(p,l)}$ is the characteristic molecular vibration frequency [9].) The factor γ_0 in the expression for bond rupture rate is an

adjustable parameter that characterizes the sensitivity of the slip bonds to the applied force. For slip bond formation in the limit of zero force, the ratio of the formation to rupture rate is given by $k_{0f}^{(l)} / k_{0r}^{(l)} = \exp(U_0^{(l)} / k_B T)$ [28,29]. In general, the rate constant of bond formation decreases under an applied force [30]. For the sake of simplicity, however, we neglect the dependence of the rate constant of bond formation on force and consider it to be constant, $k_f = k_{0f}^{(l)}$.

The evolution equation for the number of slip bonds, N_b, can be written as [3,7]:

$$\frac{dN_b}{dt} = -k_r N_b + k_f P_c(R)[N_{max}(R) - N_b]^2 \ , \qquad (5)$$

where $N_{max}(R)$ is the maximum number of bonds that can be formed and $P_c(R)$ is the probability of contact of two chain ends on two neighboring PGNs that are separated by a center-to-center distance of R [3,7]. Note that $k_f = 0$ for the permanent bonds, so that only the first term on the right-hand side of eq. (5) is used for describing the evolution of the number of permanent bonds. (The number of permanent bonds is specified at the beginning of the simulation, and since they cannot reform after they are broken, $k_f = 0$.) The specific model parameters used to characterize the bonds and their correspondence to experimental values are listed in Table 1.

The notion of a catch bond was first introduced to explain the behavior of certain biological bonds that appeared to strengthen under an applied tensile force [10]. Atomic force microscopy and biomembrane force probe experiments demonstrated that such catch bonds ruptured predominantly at either low or high applied forces and rarely at intermediate levels of force [11,13,19]. A number of phenomenological models were developed to describe the rupture of specific biochemical catch bonds under an applied force. In these models, the catch bond behavior was explained though multiple rupture pathways within a single bound state, or through

transitions between multiple bound states [13-20]. Recently, it was observed that some relatively simple chemical bonds also exhibit behavior typical of the catch bonds [21,22,31-33]. The latter behavior was attributed to the dissimilar force sensitivity of the distinct conformational states of the bond [32,33].

It is important to note that most models for catch bonds were formulated to describe the behavior of a specific biological system [18]. Our aim was to utilize a more broad-based approach, and hence, we employed a general two-state model [13,14] where the rupture behavior of a catch bond could be adjusted by varying a small set of model parameters. According to this model [13,14], a catch bond has two conformational states, state 1 and state 2 (see Fig. 2), which rupture with the force-dependent rates k_1 and k_2, respectively. The transition rates between the states, k_{12} and k_{21}, also depend on the force F. The evolution equation for number of bonds in each of the states, $N_b^{(1)}$ and $N_b^{(2)}$, can be written as (cf. eq. (5)):

$$\frac{dN_b^{(1)}}{dt} = -(k_1 + k_{12})N_b^{(1)} + k_{21}N_b^{(2)} + k_f^{(1)}P_c(R)[N_{max}(R) - (N_b^{(1)} + N_b^{(2)})]^2 \qquad (6a)$$

$$\frac{dN_b^{(2)}}{dt} = -(k_2 + k_{21})N_b^{(2)} + k_{12}N_b^{(1)} + k_f^{(2)}P_c(R)[N_{max}(R) - (N_b^{(1)} + N_b^{(2)})]^2 \qquad (6b)$$

Equations (6a) and (6b) account for evolution of the number of catch bonds in states 1 and 2 due to bond rupture, formation and transition between the states. The total number of catch bonds between two PGNs is given by the sum $N_b = N_b^{(1)} + N_b^{(2)}$.

The rupture rates in states 1 and 2 were modeled according to the Bell model as $k_1 = k_{0r}^{(l)} \exp(\gamma_1 F)$ and $k_2 = k_{0r}^{(l)} \exp(\gamma_2 F)$, respectively. To reproduce rupture behavior characteristic of the catch bonds [18,19], the force sensitivity parameters were assigned different values for the two states. In particular, $\gamma_1 = \gamma_0$ and $\gamma_2 = \gamma_0 / 3$. Hence, the rupture rate k_2 is

less sensitive than k_1 to the applied force. For the sake of simplicity, both of the bound states were assumed to have the same zero force rupture rate, $k_{0r}^{(l)}$, which is equal to that of the slip bonds.

In describing the transitions between the two states, we assumed that at zero force, the transition rates are comparable to the rupture rates. Further, we assumed that the transitions rates are biased such that 75% of the bonds are in the more force-sensitive state (state 1) at low forces, and that a rapid transition to the less force-sensitive state (state 2) occurs at finite forces. To achieve the latter behavior, the transition rates between the two states were chosen to be $k_{12} = k_{0r}^{(l)} \exp(\gamma_{12} F)$ and $k_{21} = 3k_{0r}^{(l)} \exp(\gamma_{21} F)$ at $\gamma_{12} > \gamma_{21}$. We chose these values of the rupture and transition rates to ensure that the two-state model captures the main features of the experimentally reported rupture behavior of the catch bonds [18,19].

Finally, the rate of catch bond formation is partitioned between the two states according to the equilibrium partitions, $k_{21}(k_{12} + k_{21})^{-1}$ and $k_{12}(k_{12} + k_{21})^{-1}$, established due to the inter-state transitions at a given force. At the chosen values of the transition rates, the formation rate constants for states 1 and 2 at equilibrium separation, $r_{eq} = 1.2$, are given by $k_f^{(1)} = 0.46 k_f$ and $k_f^{(2)} = 0.54 k_f$, respectively, where k_f is the formation rate constant for the slip bonds in eq. (5). Table 1 lists all the simulation parameters used to characterize the catch bonds and their correspondence to physical values.

The dynamics of the system is assumed to be in the overdamped regime, with the motion of each particle given by the equation $d\mathbf{x}/dt = \mu \mathbf{F}_{tot}$, where μ is the mobility and $\mathbf{F}_{tot}$ is the total force on the polymer-grafted particle. The total force acting on a particle can be written as $\mathbf{F}_{tot} = -\partial U_{int}/\partial \mathbf{x} + \mathbf{F}_{ext}$, where $\mathbf{F}_{ext}$ is the external force acting on the edge particles of the

particle array (see Fig. 1). This equation is solved numerically in two steps since the polymer spring force (within the expression for F_{tot}) in the dynamic equation depends on the number of bonds between particles, and consequently, on the evolution of the chemical kinetics given by eq. (5) or (6). In the first step, we determine the number of bonds at any given time, $N_b(t)$, by evolving numerically the unsteady-state kinetics, eq. (5) or (6), through an explicit Euler scheme with a time step of $10^{-2}T_0$, where T_0 is the unit of time in the simulation (see Table 1). Note that the numerical evolution of eqs. (5) and (6) yield real numbers, whereas the number of bonds $N_b(t)$ should take discrete integer values. In order to determine the integer value, we compare the fractional part of the numerical result, $\{N_b(t)\}$, with a random number ξ distributed uniformly between 0 and 1. If $\{N_b(t)\} < \xi$, then we truncate the result; otherwise, we increment the integer part of the result by 1. In the second step, we use this value for the number of bonds to calculate the spring force (see eq. (3)) in the dynamic equation and integrate numerically the resulting equation using a fourth-order Runge-Kutta algorithm with a time step of $10^{-2}T_0$.

In the ensuing simulations, we consider a particle of core radius $r_0 = 50$ nm with $f = 156$ polymer chains grafted onto its surface such that the corona of grafted arms is of thickness $H = 0.75r_0$. The value of f is used to determine the strength of the repulsion and extent of bond formation between any two interacting particles. The cohesive interaction in eq. (2) with $C = 60k_BT$, $A = 1.15\sigma$ and $B = 0.08\sigma$ counters the repulsive forces at the corona edge. The equilibrium overlap between two particles is such that for the labile bond energy of $U_0^{(l)} = 39k_BT$, the particles are separated by a center-to-center distance of $3.2r_0$ (corresponding to approximately 9% overlap) and are connected by approximately seven bonds. The motion of the particle in the overdamped regime is determined using the mobility computed as the inverse

of Stokes drag, $\mu = [6\pi\eta\, r_0(1+q)]^{-1}$, on a particle of radius $r_0(1+q)$ in a viscous fluid of viscosity $\eta = 0.894\ \mathrm{Pa}\cdot\mathrm{s}$ (viscosity of glycerol). In simulating the bond kinetics, we fix the bond energy of the permanent links to be $U_0^{(p)} = 45\,k_BT$ and examine slip and catch labile bonds with an energy of $U_0^{(l)} = 39\,k_BT$. To study the influence of the permanent bonds on the mechanical properties of the network, we vary the average number of permanent bonds between interacting particles, P, in the range $0 \le P \le 2$.

Equations (1)-(6) describe the interactions between spherical nanoparticles with a three-dimensional corona of grafted chains. In the simulations, the equations are solved on a plane through the material. Specifically, we performed strain controlled stretching on 2D dog-bone shaped samples composed of $N_{PGN} = 396$ particles and strain recovery simulations on rectangular samples composed of $N_{PGN} = 180$ particles. The central rectangular region of the dog-bone sample is composed of the same number of particles as that of the rectangular sample of dimensions 12×15 used in the strain recovery simulations.

The initial state of the system is generated using the following five-step procedure. In the first step, the nanoparticles are placed in an array such that their centers are separated by a horizontal spacing of $1.8(1+q)$ and a vertical spacing of $1.62(1+q)$, with a horizontal offset position of $0.855(1+q)$ between adjacent rows. In the second step, we hold the sample in the initial configuration for $4000\,T_0$ units of time to allow for the formation of the labile bonds. In the third step, we equilibrate the sample for a time $6000\,T_0$, during which the stressed labile bonds are broken and new bonds are formed between the adjacent PGNs according to eq. (5) or eq. (6). In the fourth step, we introduce the permanent bonds into the system. In this step, a certain number of already established labile bonds are converted randomly to permanent ones; as a

result, each pair of neighboring particles has in average of P permanent bonds. Note that P is not an integer number and can be either $P<1$ or $P\geq 1$ depending on how many permanent bonds are introduced into the network. Finally, in the fifth step, the resultant sample composed of a dual-network of permanent and labile bonds is equilibrated for 10^4 time steps, with the breakage and formation of the labile bonds being allowed.

To quantify the mechanical properties and strain recovery, eight independent runs were performed on samples at each set of model parameters. The strain ε is calculated as the ratio of the extension of the sample to its length in the undeformed state, i.e., in the state achieved in the course of the sample preparation described above.

Via our computer simulations, we employed a three-step procedure to study the strain recovery of the material. In the first step, the sample is subjected to a strain-controlled tensile deformation by pulling the left edge of the sample at a constant velocity of $v_p = 0.001$, which corresponds to roughly 3.55 nm/s, until the desired maximal value of strain, $\varepsilon_{\max}$, is reached. The values of $\varepsilon_{\max}$ were chosen to not exceed the average strain at break, ε_b. The external tensile force F acting on the left edge of the sample is recorded as a function of ε during the first step. In the second step, the force F is relaxed to zero at a constant rate over the time $10^4 T_0$, and the strain ε is recorded (force-controlled strain relaxation). The inelastic component of the deformation is characterized by the residual strain, ε_0, which is recorded at the moment of time when $F = 0$. Finally, in the third step of the procedure, the relaxation of the residual strain at zero external force is tracked over some period of time. To elucidate the mechanism of strain recovery, the samples are subject to either single or multiple cycles of the stretching and relaxation procedure.

III. Results and Discussion

A. Rupture behavior of the slip and catch bonds

In our previous studies of PGNs bound by slip bonds [3-7], we found that the mechanical properties of the network (i.e., ductility, toughness, and strain recovery) were dependent on the rate of the applied strain. Before investigating the behavior of the new networks, it is instructive to first consider the effect of the strain rate on just two PGNs that are bound by catch bonds. In these simulations, the bound particles are pulled apart at a constant velocity, and we contrast the rupture rate of individual slip and catch bonds for various pulling velocities.

For a single polymer arm, the probability, p, of forming a slip bond is given by [7]:

$$\frac{dp}{dt} = -k_r p + k_f P_c(R)[N_{max}(R) - N_b](1-p) \quad , \tag{7}$$

where the total number of bonds between the two PGNs, N_b, is determined by eq. (5). Similarly, the probabilities, p_1 and p_2, of forming a catch bond in states 1 and 2, respectively, are given by:

$$\frac{dp_1}{dt} = -(k_1 + k_{12})p_1 + k_{21}p_2 + k_f^{(1)} P_c(R)[N_{max}(R) - N_b](1-p_1-p_2) \quad , \tag{8a}$$

$$\frac{dp_2}{dt} = -(k_2 + k_{21})p_2 + k_{12}p_1 + k_f^{(2)} P_c(R)[N_{max}(R) - N_b](1-p_1-p_2) \quad , \tag{8b}$$

where the number of bonds, $N_b = N_b^{(1)} + N_b^{(2)}$, is determined by solving eq. (6). The probability of having a catch bond in either of the two states is given by the sum $p = p_1 + p_2$. The effect of pulling the two particles apart is modeled through eqs. (5)-(8) by the introduction of the time-dependent inter-particle distance $R = R_{eq} + vt$, where v is the pulling velocity, and R_{eq} is the initial particle separation, which is taken to be the equilibrium distance between the two particles. Note that R_{eq} is different for the slip and catch bonds.

The pulling velocity v was varied in the range from $0.05v_p$ to $5v_p$, where $v_p = 0.001$ corresponds to a velocity of approximately 3.55nm/s. The latter value is typical for single molecule pulling experiments [34]. At $v = v_p$, the bond rupture rate at zero force, k_{0r}, is lower than the strain rate, $v_p R_{eq}^{-1}$, by approximately two orders of magnitude [4]. Correspondingly, the strain rate, $v R_{eq}^{-1}$, spans the range from $5k_{0r}$ to $500k_{0r}$ within the chosen range of v.

Figure 3 shows the value of $(-dp/dt)$ as a function of strain, $\varepsilon = R R_{eq}^{-1} - 1$, calculated for the slip and catch bonds. We use the term "rupture rate" for the value $(-dp/dt)$ because, as a function of ε, this value is proportional to the probability of a bond rupturing within the interval of strains from ε to $\varepsilon + d\varepsilon$. Figure 3a depicts the rupture rates of the slip and the catch bonds between two PGNs at the pulling velocities of $0.2v_p$, v_p, $5v_p$. The rupture rates for the slip bonds exhibit a single maximum (dashed lines), whereas those for the catch bonds display two maxima separated by a minimum (solid lines).

The single maximum of the slip bonds arises due to the single energy barrier separating the bound and unbound states. This maximum in the rupture rate is seen to shift towards larger strains with an increase in the strain rate (Fig. 3a). The latter behavior is consistent with observations that the slip bonds can withstand progressively larger forces under increasing loading rates [18].

The two maxima observed in the rupture rates of the catch bonds correspond to rupturing the two individual bound states. Figure 3a indicates that with an increase in the strain rate, the peaks shift towards greater strains and become more separated so that the probability of rupture decreases at the intermediate values of strain. Moreover, at sufficiently high strain rates, the transition to the less force-sensitive bound state is accelerated and the high-strain maximum in

the rupture rate becomes more pronounced (Fig. 3a). Hence, it is evident that the two-state model used here is capable of reproducing the rupture behavior associated with the notion of catch bonds [18,19].

The difference between the rupture behavior of the slip and catch bonds becomes less pronounced as the strain rate decreases. Figure 3b shows the rupture rates for the two types of bonds at the pulling velocity of $0.05v_p$. The maximal rate of rupture of the catch bond (solid line) takes place at approximately the same value of strain as that for the slip bond (dashed line). The high-strain peak observed for the catch bond at higher strain rates (see the solid lines in Fig 3a) has now been reduced to a wide shoulder, as indicated by the solid line in Fig 3b. We can conclude, therefore, that close to the mechanical equilibrium at zero force, the slip and catch bonds exhibit similar rupture behavior, and that the response to the applied force characteristic of the catch bonds becomes prominent only at sufficiently high strain rates.

B. Ductility and toughness of networks bound by slip and catch bonds

To elucidate the effect of the bond type (slip or catch) on the mechanical properties of the PGN network, we modeled the strain-controlled tensile deformation of dog-bone shaped samples composed of $N_{\mathrm{PGN}} = 396$ particles. The samples were stretched at a fixed strain rate until they ruptured. The strain, ε, was calculated as the ratio of the extension of the sample to its original length. The force required to stretch the sample and the number of bonds in the network were recorded in the course of the deformation.

We first consider scenarios where the interconnections are all labile bonds, i.e., there are no permanent bonds in the system and thus, $P = 0$. Recall that the permanent bonds are modeled as slip bonds, and thus, for $P \neq 0$, even networks involving the catch bonds encompass some slip bonds. With $P = 0$, however, the networks are formed from either all slip or all catch bonds.

Figures 4a and 4b show force versus strain curves obtained from simulations of the respective networks at pulling velocities of $0.2v_p$, $1v_p$ and $5v_p$. The resistance of the samples to tensile deformation (i.e., force) increases with the strain rate for both the slip and catch bond networks. Notably, the force profiles of the two different networks are similar below the yield point. Moreover, the yield strain is the same for both types of networks ($\varepsilon \approx 0.15$) and is not affected by the strain rate. After the yield point ($\varepsilon > 0.15$), the force-strain behavior of the two networks appear to be quite different, as can be seen by comparing Fig. 4a (slip bond network) and Fig. 4b (catch bond network). At the higher pulling velocities of $1v_p$ and $5v_p$, the slip bond network breaks at lower strains ($\varepsilon < 0.75$) than the catch bond network ($\varepsilon > 1.0$). Additionally, the force-at-break for the catch bond network ($40 < F/F_0 < 100$) is a factor of two greater than that for the slip bond network ($20 < F/F_0 < 40$).

During the course of the imposed tensile deformation, stretched labile bonds rupture and new bonds form, leading to structural rearrangements in the sample. Figures 4c and 4d show the evolution of the number of bonds per particle, N_b / N_{PGN}, as a function of strain, ε, for the respective slip and the catch bond networks. The behavior of N_b / N_{PGN} clearly depends on both the strain and the strain rate. Specifically, at small strains ($\varepsilon < 0.25$), we observe a pronounced reduction in N_b / N_{PGN} at the lowest pulling velocity ($0.2v_p$). The latter reduction in N_b / N_{PGN} is less pronounced at the velocity of $1v_p$ and vanishes at the highest velocity of $5v_p$ for both the slip and catch bond networks. Correspondingly, samples having more bonds provide greater resistance to the initial deformation, as can be seen in Figs. 4a and 4b.

At larger strains of $\varepsilon \geq 0.25$, the values of N_b / N_{PGN} remain either constant or increase, indicating that the deformation induces bond formation (see Figs 4c and 4d). In our prior studies

[3], we showed that such bond formation occurs predominantly in the direction normal to the stretching direction. The bonds thus formed are not expected to resist tensile deformation of the network, so the enhanced resistance at larger strains and strain rates occurs due to the survival of the stretched bonds. Specifically, in the catch bond network, the transition to high-strain ruptures at larger strain rates (see Fig. 3a) enhances the survival of stretched bonds, and consequently, the resistance to deformation at larger strains (see Fig 4b).

The addition of the permanent bonds was shown to enhance the mechanical properties of the networks formed by weak, labile slip bonds [3]. Here, we used force-strain curves similar to those in Figs. 4a and 4b to obtain the strain at break, ε_b, and toughness, W, of networks having an average number of permanent bonds, P, per bonded pair. The strain at break, ε_b, is a measure of the ductility of sample and was determined by the strain at which the resistance to deformation drops as the sample fractures. The toughness, W, is defined here as the work-to-break per particle and was determined by integrating the force-strain curve, and dividing the resulting value by the number of nanoparticles in the sample, N_{PGN}. Figure 5 shows the strain at break (Figs. 5a and 5b) and the toughness (Figs. 5c and 5d) at three different strain rates as a function of average number of permanent bonds per pair, P, introduced into the slip (Figs 5a and 5c) and catch (Figs. 5b and 5d) bond networks. The data points and error bars shown are obtained using Weibull statistics [36] on data from eight independent simulation runs.

Figure 5 shows that introduction of the permanent bonds has almost no effect on ε_b and W in both the slip and catch bond networks as these values exhibit little change when the number of permanent bond is increased from $P = 0$ to $P = 2$. The strain at break and toughness of a network are seen to be determined mostly by the type of bond (slip or catch) and the strain rate. Notably, at $v = 5v_p$ and $P = 0$, the average strain at break and toughness for the catch bonds

network are approximately 90% and 165% greater, respectively, than those for the slip bond network. Such a pronounced effect of the catch bonds on the ductility and toughness of a network can be attributed to shifting the rupture rate towards higher strains at a high strain rate (see red solid curve in Fig. 3a).

We can obtain further insight on the relationship between the bond type and the mechanical properties of the network by examining snapshots of the samples with no permanent bonds ($P = 0$). Figures 6a and 6b show snapshots of the slip and the catch bond networks, respectively, at $P = 0$ at the strain of $\varepsilon \approx 0.50$ achieved with a pulling velocity of $1 v_p$. In the slip bond network (Fig. 6a), we observe the onset of failure through the formation of voids. In contrast, the catch bond network (Fig. 6b) appears to be intact and relatively homogeneous at this strain. To quantify the heterogeneity of the slip and the catch networks, we examined the distribution of bonds in the central rectangular region of dimensions 12×15 particles in the dog-bone shaped sample. Figure 6c shows the distribution of number of bonds between the bonded pairs in this central region. The catch bond network is seen to exhibit from 1 to 11 bonds per pair, with a pronounced maximum at 6-8 bonds per pair. In comparison, the slip bond network shows a broader distribution of number of bonds, i.e., from 1 to 15 bonds per pair. The observed increase in number of pairs with more than 10 bonds indicates clustering in the slip bond networks. Thus, the survival of stretched bonds in the catch bond networks not only prevents void formation, but also seems to prevent clustering. The reduced heterogeneity of the catch bond networks is expected to play an important role in strain recovery and rejuvenation when the force on the network is released.

C. Hysteresis and strain recovery in slip and catch bond networks

In the previous section, we demonstrated that under tensile deformation, the ductility and toughness of networks bound by catch bonds are distinctly different from those for networks that are interconnected slip bonds. A particular aim of these studies is to determine how these systems recover when the applied force is released. Namely, if the force is released before the networks break, structural changes induced by the deformation can potentially be reversed and thus, the system can recover from the applied tensile force. In this manner, the systems can exhibit a degree of self-healing. To quantify this process, we calculate the hysteresis and strain recovery in the slip and catch bond networks that occurs once the force is released at the maximum strain of $\varepsilon_{\max} = 0.5$ (see Methodology). For these simulations, we used rectangular samples of size 12×15 units that are identical to the central rectangular regions of the dog-bone shaped samples used in the previous section.

Figures 7a and 7b show the force-strain curves obtained from simulations of strain recovery in the slip and catch bond networks at $P = 0$ and $P = 2$, respectively. Using these plots, we calculated the value of the hysteresis, ΔW, as the area enclosed by the force-strain curves; ΔW is a measure of energy dissipated in the system as it undergoes the loading and unloading of the applied force. The catch bond networks clearly exhibit a smaller hysteresis than the slip bond networks (Figs. 7a and 7b). The latter behavior indicates that the contribution of irreversible processes in the deformation of catch bond networks is smaller than that in the case of the slip bond networks. Specifically, at $P = 0$ (no permanent bonds, Fig. 7a), the average value of the hysteresis in the catch bond networks (ΔW = 5.95) is approximately 2.2 times smaller than that in the slip bond networks (ΔW = 13.28). The introduction of the permanent bonds results in a reduction of the hysteresis (as can be seen by comparing Figs. 7a and 7b). At $P = 2$, the average values of hysteresis observed in the slip and catch bond networks were $\Delta W = 10.98$ and 4.11,

respectively. It is note worthy that the type of labile bond (slip or catch) has a stronger effect on the value of hysteresis than the presence of permanent bonds in the network (Figs. 7a and 7b).

Figures 7c and 7d demonstrate that the residual strain, ε_0, is also more sensitive to the type of labile bond (slip or catch) than to the presence of permanent bonds. The value of ε_0 indicates the strain in the system when the applied force has relaxed to zero. The catch bond networks exhibit a negligibly small residual strain at both $P = 0$ and $P = 2$ (see the blue lines in Figs. 7c and 7d). In contrast, the residual strain in the slip bond networks is $\varepsilon_0 \approx 0.29$ at $P = 0$. While the introduction of the permanent bonds at $P = 2$ results in a two-fold reduction in ε_0 for the slip bond case, this value of ε_0 is still higher than the corresponding value for the catch bond system (see Figs. 7c and 7d) .

After repeated deformation, irreversible changes in the network structure can accumulate and result in the progressive deterioration of the material's mechanical properties. To elucidate how the type of labile bond (slip or catch) affects the recovery processes after repeated applications of the tensile force, we modeled the behavior of the slip and catch bond networks at $P = 0$ (no permanent bonds) under multiple cycles of straining and relaxation. In each cycle, we imposed a strain-controlled tensile deformation at a constant pulling velocity of $1v_p$; this was followed by the release of the force at a constant rate during a period of time equal to $10^4 T_0$ and relaxation at zero force for $5 \times 10^4 T_0$. We considered the two types of cyclic deformation shown schematically in Fig. 8. For type I cyclic deformation, we imposed the same maximal strain of $\varepsilon_{\max} = 0.5$ in five consecutive cycles (Fig. 8a). For type II deformation, we increased the maximal strain in the five consecutive cycles from $\varepsilon_{\max} = 0.1$ to 0.5 in steps of 0.1 (Fig. 8b).

Figures 9a and 9b display the force–strain curves obtained from modeling the type I cyclic deformation of the slip and the catch bond networks, respectively. The behavior of the material under repeated deformation is significantly dependent on the type of bond (slip or catch) forming the network (Figs. 9a and 9b). In the ensuing discussion, the loading curve refers the tensile force as a function of strain during the strain-controlled loading and similarly, the unloading curve refers to the tensile force observed during the force release. Notably, in the slip bond network, the loading curve closely follows the unloading curve from the previous cycle (Fig. 9a). This behavior indicates that structural changes, which occurred within the network during each deformation up to the maximal strain $\varepsilon_{\max} = 0.5$, could not be reversed during the unloading and relaxation stages of a deformation cycle. Most of the irreversible changes in the slip bond network took place during the first cycle of deformation. The latter behavior is evident from Figs. 9c and 9d, which show the respective average values of the residual strain, ε_0, and hysteresis, ΔW, as functions of the number of deformation cycles,. After the significant changes incurred during the first cycle, subsequent cycles yielded only a slight increase in the residual strain (the green line in Fig. 9c) and the hysteresis remains low (green line in Fig. 9d).

In contrast to the slip bond network, irreversible structural changes occurring within the material accumulate relatively gradually for catch bond networks under cyclic deformation. Figure 9b shows that the loading and unloading curves look similar for the first two cycles of deformation of the catch bond network, and it is only after the third round of stretching and relaxation that the loading curves follow the unloading ones of a previous cycle (Fig. 9b). Correspondingly, for the catch bond network, the values of the residual strain are relatively small and exhibit a gradual increase; the hysteresis displays a gradual decrease (blue curves in Figs. 9c and 9d).

By modeling type II cyclic deformations (Fig. 8b), we could establish the onset of irreversible structural changes as the maximal strain is increased. Figures 10a and 10b show the force–strain curves obtained from five consecutive cycles of the type II deformation of the slip and catch bond networks, respectively. Both the slip and catch bond networks exhibit complete recovery after the first three consecutive cycles when the maximal strain is $\varepsilon_{\max} \leq 0.3$. The loading curves follow the same path (Figs. 10a and 10b), and no residual strain is observed in both of the networks (Fig. 10c) after loading and relaxation at $\varepsilon_{\max} \leq 0.3$. These properties are clear indications of the material's complete recovery. The hysteresis (i.e., energy dissipation) is, however, smaller in the catch bond network than that in the network formed by the slip bonds (Fig. 10d).

When the maximal strain was increased to $\varepsilon_{\max} = 0.4$, irreversible changes did take place in the slip bond network. The material exhibits a notable residual strain after the fourth cycle (green curve in Fig. 10c), and the initial part of the loading curve of the fifth cycle of deformation follows the unloading curve of the fourth cycle (Fig. 10a). In contrast, Fig. 10b shows a robust recovery of the catch bond networks during all five consecutive cycles of stretching and relaxation. A slight indication of the onset of irreversible deformations in the catch bond networks after stretching up to $\varepsilon_{\max} = 0.5$ is, however, seen in Fig. 10c (blue curve), which reveals the existence of small but non-zero residual strain after the fifth cycle of deformation.

Conclusions

One of our aims in modeling PGN networks was to design materials that exhibit a pronounced ability to both resist and recover from mechanical deformation. Inspired by the performance of biological catch bonds, which can become stronger under an applied force, we

developed a computational model that allowed us to simulate the mechanical behavior of PGNs that are interconnected by labile catch bonds, which can reform after they have ruptured. By comparing the performance of PGN networks that are bound by slip bonds to those bound by catch bonds, we could establish the utility of the catch bonds in improving the mechanical response of the material to an applied tensile force.

In carrying out these studies, we built on our prior simulations of dual cross-linked PGN networks that were interconnected by two types of slip bonds: labile and permanent. The permanent bonds are stronger and less reactive than the labile bonds, and thus, do not reform after they are broken. We previously found that the permanent bonds provided a "backbone" that helped maintain the structural integrity of the network and promoted the self-healing of the material as it was being strained [3,4]. Hence, in the present studies, we also considered scenarios involving such dual cross-linked systems.

Focusing on networks that contained just the slip bonds, we found that increasing the average number of permanent bonds, P, between a pair of particles led to improvements in the ductility and toughness of the network. The effects of increasing P, however, proved to be relatively small compared to the changes that resulted when the labile slip bonds where replaced by labile catch bonds. This change in bond type yielded dramatic improvements in the ductility and toughness. In other words, changing the slip to catch bonds had a more significant effect than increasing P within the slip bond network on the ability of the material to resist mechanical deformation.

In the above studies, the materials' resistance to deformation depended on the strain rate for the catch bond networks, showing more marked effects at faster strain rates. We correlated

this behavior to the decrease in the rupture rate of catch bonds with an increase in the rate of strain.

We also simulated the behavior of the networks when the applied tensile force was released and the network was allowed to relax to zero applied force. These simulations allowed us to characterize the strain recovery in the system (i.e., the residual strain at zero force) and the hysteresis. The hysteresis indicates the energy dissipation within the system and is a measure of the irreversible structural damage within the material. By examining the performance of the materials under single and multiple cycles of deformation (loading and unloading of the force), we found that networks cross-linked with catch bonds exhibited enhanced strain recovery (less residual strain) and exhibited a pronounced reduction in hysteresis relative to the slip bond networks. These results indicate that the introduction of catch bonds led to less deterioration in the material than is present in the slip bond networks. Namely, the increase in bond lifetimes brought about by the catch bonds curtailed irreversible and detrimental restructuring of the network, such as the formation of voids.

We also found that the onset of irreversible restructuring in the catch bond networks occurred at a larger strain than in the slip bond networks. The latter response of the catch bond networks is due to the ability of the catch bonds to transition to a less force-sensitive state that allows for enhanced survival of these bonds at large strain.

In summary, the results of these studies reveal that the catch bonds are useful for enhancing the ductility and toughness of the PGN networks; these improvements are due to catch bonds forestalling catastrophic failure of these materials under tensile deformation. The findings also highlight that the networks interconnected by catch bonds are resistant to fatigue as they withstand multiple cycles of deformation and thus, exhibit enhanced durability. These

predictions provide valuable guidelines for fabricating a new class of mechanically robust nanocomposites through the incorporation of biomimetic catch bonds.

Acknowledgements

ACB gratefully acknowledges financial support from the DOE (for partial support of BVSI) and AFOSR (for partial support of VVY) and helpful conversations with Prof. Dan Hammer.

References

1. Kolmakov GV, Matyjaszewski K, Balazs AC. Harnessing labile bonds between nanogel particles to create self-healing materials. ACS Nano 2009;3:885-892. DOI: 10.1021/nn90052h
2. Salib IG, Kolmakov KV, Gnegy CN, Matyjaszewski K, Balazs AC. Langmuir 2011;27:3991-4003. DOI:10.1021/la104609t
3. Iyer BVS, Salib IG, Yashin VV, Kowalewski T, Matyjaszewski K, Balazs AC. Modeling the response of dual cross-linked nanoparticle networks to mechanical deformation. Soft Matter 2013;9:109-21. DOI: 10.1039/c2m27121d
4. Iyer BVS, Yashin VV, Kowalewski T, Matyjaszewski K, Balazs AC. Strain recovery and self-healing in dual cross-linked nanoparticle networks. Polym Chem 2013;4:4927-39. DOI: 10.1039/c3py00075c
5. Hamer MJ, Iyer BVS, Yashin VV, Kowalewski T, Matyjaszewski K, Balazs AC. Modeling polymer-grafted nanoparticles reinforced by high strength chains. Soft Matter 2013;10:1374-83. DOI: 10.1039/c3sm52300d

6. Iyer BVS, Yashin VV, Balazs AC. Dynamic behavior of dual cross-linked nanoparticle networks under oscillatory shear. New J Phys 2014;16:(0750009) 1-26. DOI: 10.1088/1367-2630/16/7/075009

7. Iyer BVS, Yashin VV, Hamer MJ, Kowalewski T, Matyjaszewski K, Balazs AC. Ductility, toughness and strain recovery in self-healing dual cross-linked nanoparticle networks studied by computer simulations. Prog Polym Sci 2014. DOI: 10.1016/j.progpolymsci.2014.07.004

8. Hamer MJ, Iyer BVS, Yashin VV, Balazs AC. Designing mechanomutable composites: reconfiguring the structure of nanoparticle networks through mechanical deformation. DOI: 10.1021/nl501871e

9. Bell GI. Models for the specific adhesion of cells to cells. Science 1978;200**:**618-27. DOI: 10.1126/science.347575

10. Dembo M, Torny DC, Saxman K, Hammer D. The reaction-limited kinetics of membrane-to-surface adhesion and detachment. Proc R Soc Lond B 1988;234:55-83. DOI: 10.1098/rspb.1988.0038

11. Marshall BT, Long M, Piper JW, Yago T, McEver RP, Zhu C. Direct observation of catch bonds involving cell-adhesion molecules. Nature 2003;423:190-93. DOI: 10.1038/nature01605

12. Yago T, Wu J, Wey D, Klopocki AG, Zhu C, McEver R P. Catch bonds govern adhesion through L-selectin at threshold shear. J Cell Biol 2004;166:913-23. DOI: 10.1083/jcb.200403144

13. Evans E, Leung A, Heinrich V, Zhu C. Mechanical switching and coupling between two dissociation pathways in P-selectin adhesion bond. Proc Natl Acad Sci USA 2004;101:11281-86. DOI: 10.1073/pnas.0401870101

14. Barsegov V, Thirumalai D. Dynamics of unbinding of cell adhesion molecules: transition from catch to slip bonds. Proc Natl Acad Sci USA 2005;102:1835-39. DOI: 10.1073/pnas.0406938102

15. Hammer DA. Leukocyte adhesion: what's the catch? Curr Biol 2005;15:R96-99 .

16. Perverzev YV, Prezhdo OV, Forero M, Sokurenko EV, Thomas WE. The two-pathway model for the catch-slip transition in biological adhesion. Biophys J 2005;89:1446-54. DOI: 10.1529/biophysj.105.062158

17. Pereverzev YV, Prezhdo OV. Force-induced deformation and stability of biological bonds. Phys Rev E 2006;73, 050902R1-4. DOI: 10.1103/PhysRevE.73.050902

18. Thomas WE, Vogel V, Sokurenko E. Biophysics of catch bonds. Ann Rev Biophys 2008;37:399-416. DOI: 10.1146/annurev.biophys.37.032807.125804

19. Thomas W. Catch bonds in adhesion. Ann Rev Biomed Eng 2008;10:39-57. DOI:10.1146/annurev.bioeng.10.061807.160427

20. Prezhdo OV, Pereverzev YV. Theoretical aspects of the biological catch bond. Acc of Chem Res 2009;42(6):693-703. DOI: 10.1021/ar800202z

21. Konda SSM, Brantley JN, Varghese BT, Wiggins KM, Bielawski CW, Makarov DE. Molecular catch bonds and the anti-hammond effect in polymer mechanochemistry. J Am Chem Soc 2013;135:12722-29. DOI: 10.1021/ja40511081

22. Groote R, Szyga BM, Laibfarth FA, Hawker CJ, Doltsinis NA, Sijbesma RP. Strain-induced strengthening of the weakest link: the importance of intermediate geometry for the outcome of mechanochemical reactions. Macromolecules 2014;47:1187-92. DOI: 10.1021/ma4022339

23. Likos CN, Löwen H, Watzlawek M, Abbas B., Jucknischke O, Allgaier J, Richter D. Star polymers viewed as ultrasoft colloidal particles. Phys Rev Lett 1998;80:4450-53. DOI: 10.1103/PhysRevLett.80.4450

24. Jusufi A, Watzlawek M, Löwen H. Effective interaction between star polymers. Macromolecules 1999;32:4470-73. DOI: 10.1021/ma981844u

25. Daoud M, Cotton JP. Star shaped polymers: a model for the conformations and its concentration dependence. J Phys (Paris) 1982;43:531-38. DOI: 10.1051/jphys:0198200430353100

26. Lo Verso F, Likos CN, Reatto L. Star polymers with tunable attractions: cluster formation, phase separation, reentrant crystallization. Progr Colloid Polym Sci 2006;133:78-87. DOI: 10.1007/2882_067

27. Dobrynin AV, Carrillo YJ. Universality in nonlinear elasticity of biological and polymeric networks and gels. Macromolecules 2011;44:140-46. DOI: 10.1021/na102154u

28. Bell GI, Dembo M, Bongrad P. Competition between nonspecific repulsion and specific bonding. Biophys J 1984;45:1051-64. DOI: 10.1016/S0006-3495(84)84252-6

29. Bhatia SK, King MR, Hammer DA. The state diagram for cell adhesion mediated by two receptors. Biophys J 2003;84:2671-90. DOI: 10.1016/S0006-3495(03)75073-5

30. Diezemann G, Janshoff A. Dynamic force spectroscopy: analysis of reversible bond-breaking dynamics. J Chem Phys 2008;129:084904-1-10. DOI:10.1063/1.2968543

31. Akbulatov S, Tian Y, Kapustin E, Boulatov R. Model studies of the kinetics of ester hydrolysis under stretching force. Angew Chem Int Ed 2013;52:6992-95. DOI: 10.1002/anie.201300746

32. Garcia-Manyes S, Liang J, Szoszkeiewicz R, Kuo T, Fernández JM. Force-activated reactivity switch in a bimolecular chemical reaction. Nature Chem 2009;1:236-42. DOI: 10.1038/NCHEM.207

33. Dopieralski P, Ribas-Arino J, Anjukandi P, Krupicka M, Kiss J, Marx D. The Janus-faced role of external forces in mechanochemical disulfide cleavage. Nature Chem 2013; 5:685-91. DOI: 10.1038/NCHEM.1676

34. Wiita AP, Ainavarapu SRK, Huang HH, Fernandez JM. Force-dependent chemical kinetics of disulfide bond reduction observed with single-molecule techniques. Proc Natl Acad Sci USA 2006; 103: 7222-7227. DOI: 10.1073/pnas.0511035103.

35. Lawn BR. Fracture of brittle solids. Cambridge University Press, New York, 2nd edn, 1993

Figure Captions

Fig. 1. Polymer grafted nanoparticles (PGNs) consist of a rigid core (drawn in dark blue) and a corona of end-functionalized polymers. (To highlight the chain ends, the region encompassing these ends is indicated in the lightest shade.) With the overlap between neighboring coronas, the reactive end groups can form labile or permanent bonds (indicated in green) that connect the polymer arms (in solid red) and thus, link the particles. PGNs interlinked by both labile and permanent bonds form a dual cross-linked nanoparticle network.

Fig. 2. Rupture of the slip and catch bonds. Slip bonds have one bound state; the bond rupture rate is given by $k_r(F)$, which depends on the force F. Catch bonds have the two bound states, state 1 and state 2; the respective rupture rates are given by $k_1(F)$ and $k_2(F)$. Rate constants for the transitions between the bound states, $k_{12}(F)$ and $k_{21}(F)$, are also force-dependent.

Fig. 3. Rupture rate, $(-dp/dt)$, as a function of strain, ε, for slip (dashed lines) and catch (solid lines) bonds between two polymer grafted nanoparticles at the pulling velocities of: (a) $0.2v_p$ (green), v_p (blue) and $5v_p$ (red), and (b) $0.05v_p$ (black).

Fig. 4. Force, F/F_0, as a function of strain, ε, for networks cross-linked by the following labile bonds: (a) slip and (b) catch. Number of labile bonds per particle, N_b/N_{PGN}, as a function of strain, ε, for networks cross-linked by the following bonds: (c) slip and (d) catch. Dog-bone shaped samples were composed of $N_{\mathrm{PGN}} = 396$ particles, cross-linked by just labile bonds ($P = 0$), and stretched at the pulling velocities of $0.2v_p$ (green curves), v_p (blue curves) and $5v_p$ (red curves). Plots show the results from a single simulation run for each of the different cases.

Fig. 5. Average strain at break, ε_b, as a function of the average number of permanent bonds per bound pair, P, for networks cross-linked by the following labile bonds: (a) slip and (b) catch. Average toughness, W, as a function of average number of permanent bonds per bound pair, P, for the networks cross-linked by the following labile bonds: (c) slip and (d) catch. Dog-bone shaped networks were composed of $N_{\mathrm{PGN}} = 396$ particles and stretched at the pulling velocities of $0.2v_p$ (green curves), v_p (blue curves) and $5v_p$ (red curves). Averaging was performed over eight independent runs.

Fig. 6. Snapshots of the dog-bone shaped samples at strain of $\varepsilon = 0.5$. (a) Slip bond network. (b) Catch bond network. (c) Distribution of the number of bonds between two neighboring PGNs

within the central region of the samples (region delineated by the dashed lines in (a) and (b)). Green and blue bars correspond to the slip and catch labile bond networks, respectively. Samples contained no permanent bonds ($P=0$), and were stretched at the pulling velocity of v_p.

Fig. 7. Force-strain curves in the course of loading, unloading, and relaxation at zero force as obtained from a single simulation run for PGN networks cross-linked by the slip (green curves) and catch (blue curves) bonds at the average number of permanent bonds of: (a) $P=0$, and (b) $P=2$. Average strain, ε, as a function of time, Δt, in the course of unloading and relaxation at zero force as obtained from eight independent simulations of the slip (green curves) and catch (blue curves) networks at: (c) $P=0$ and (d) $P=2$. Dashed lines in (c) and (d) indicate the moments of time when the external force is completely relaxed ($F=0$). Rectangular-shaped networks were composed of $N_{\mathrm{PGN}}=180$ particles.

Fig. 8. Schematics of (a) type I and (b) type II cyclic tensile deformations of the PGN networks.

Fig. 9. Force-strain curves obtained from one run of the simulations of cyclic type I deformation of the following: (a) slip and (b) catch bond networks. Line colors correspond to the consecutive deformations as shown in Fig 8a. Averaged values of (c) residual strain and (d) hysteresis as functions of the number of cycles obtained from eight independent simulations of the type I cyclic deformation of the slip (green curves) and catch (blue curved) bond networks. Rectangular samples were composed of $N_{\mathrm{PGN}}=180$ particles and contained no permanent bonds ($P=0$).

Fig. 10. Force-strain curves obtained from one run of simulations of type II cyclic deformation of the (a) slip and (b) catch bond networks. Line colors correspond to the consecutive deformations as shown in Fig 8b. Averaged values of (c) residual strain and (d) hysteresis as functions of the number of cycles obtained from eight independent simulations of the type II cyclic deformation of the slip (green curves) and catch (blue curved) bond networks. Rectangular samples were composed of $N_{\mathrm{PGN}} = 180$ particles and contained no permanent bonds ($P = 0$).

Table 1. Parameters used in the simulations

Dimensional units				
Length: nanoparticle radius	r_0 = 50 nm			
Time, t	T_0 = 1.41×10^{-2} s			
Velocity, v	$v_0 = r_0 T_0^{-1}$ = 3.55 μm/s			
Force, F	F_0 = 2.98 pN			
Toughness, W	$F_0 r_0$ = 89.74 kJ/mol			
Bond parameters	Catch bond state 1	Catch bond state 2	Slip bond	Permanent bond (slip)
Bond energy, U_0	$39k_BT$	$39k_BT$	$39k_BT$	$45k_BT$
Rupture rate at F =0, k_{0r}	$1.62\times10^{-6}T_0^{-1}$	$1.62\times10^{-6}T_0^{-1}$	$1.62\times10^{-6}T_0^{-1}$	$4.03\times10^{-9}T_0^{-1}$
Transition rate at F =0, $k^0_{I\to F}$	$1.62\times10^{-6}T_0^{-1}$	$4.86\times10^{-6}T_0^{-1}$	0	0
Formation rate, k_{0f}	$\frac{k_{21}}{k_{12}+k_{21}}30T_0^{-1}$	$\frac{k_{12}}{k_{12}+k_{21}}30T_0^{-1}$	$30T_0^{-1}$	0
Bond sensitivity, γ	$6F_0^{-1}$	$2F_0^{-1}$	$6F_0^{-1}$	$6F_0^{-1}$
Transition sensitivity, $\gamma_{I\to F}$	$6F_0^{-1}$	$1.6F_0^{-1}$	$6F_0^{-1}$	$6F_0^{-1}$
Characteristics of polymer grafted nanoparticle (PGN)	Corona thickness $H = 0.75r_0$		Corona thickness $H = 1.25r_0$	
Kuhn length, l_p	1 nm			
Number of grafted arms, f	156			
Arm contour length, L	$8.89r_0$		$16.35r_0$	
Chain spring constant, κ_0	$7.81\times10^{-2}F_0r_0^{-1}$		$4.25\times10^{-2}F_0r_0^{-1}$	
Repulsion parameter σ	$3.02r_0$		$3.88r_0$	
Cohesion parameter A	1.15σ			
B	0.08σ			
C	$60k_BT$			
Mobility of PGN, μ	$0.57v_0F_0^{-1}$		$0.44v_0F_0^{-1}$	
Pulling velocity, v	$2\times10^{-4}v_0$, $1\times10^{-3}v_0$, and $5\times10^{-3}v_0$			

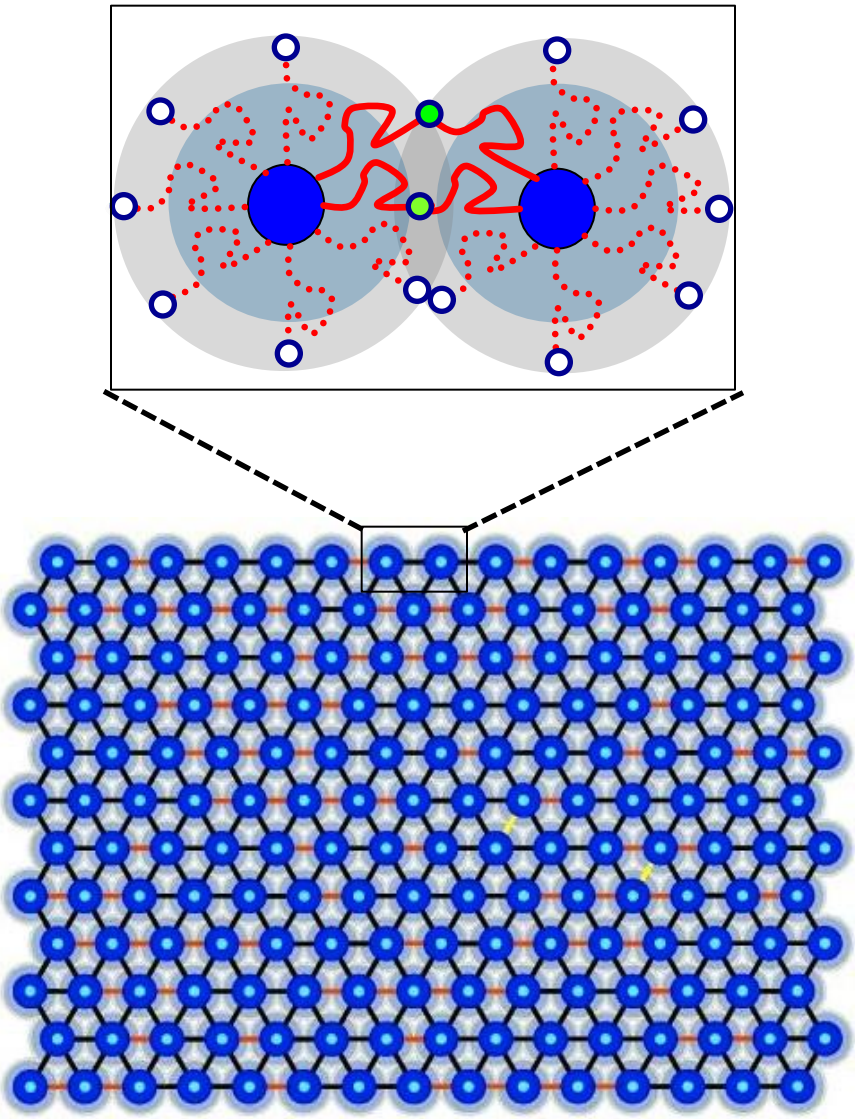

Fig. 1

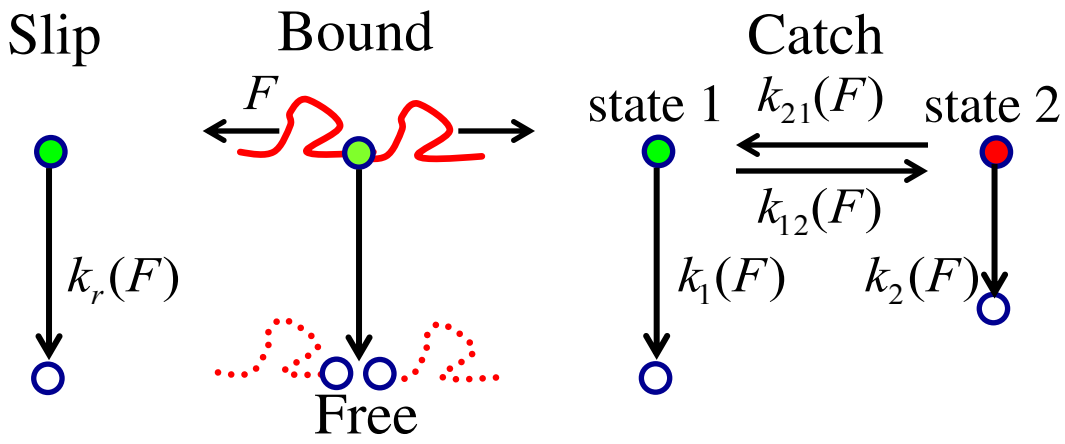

Fig. 2

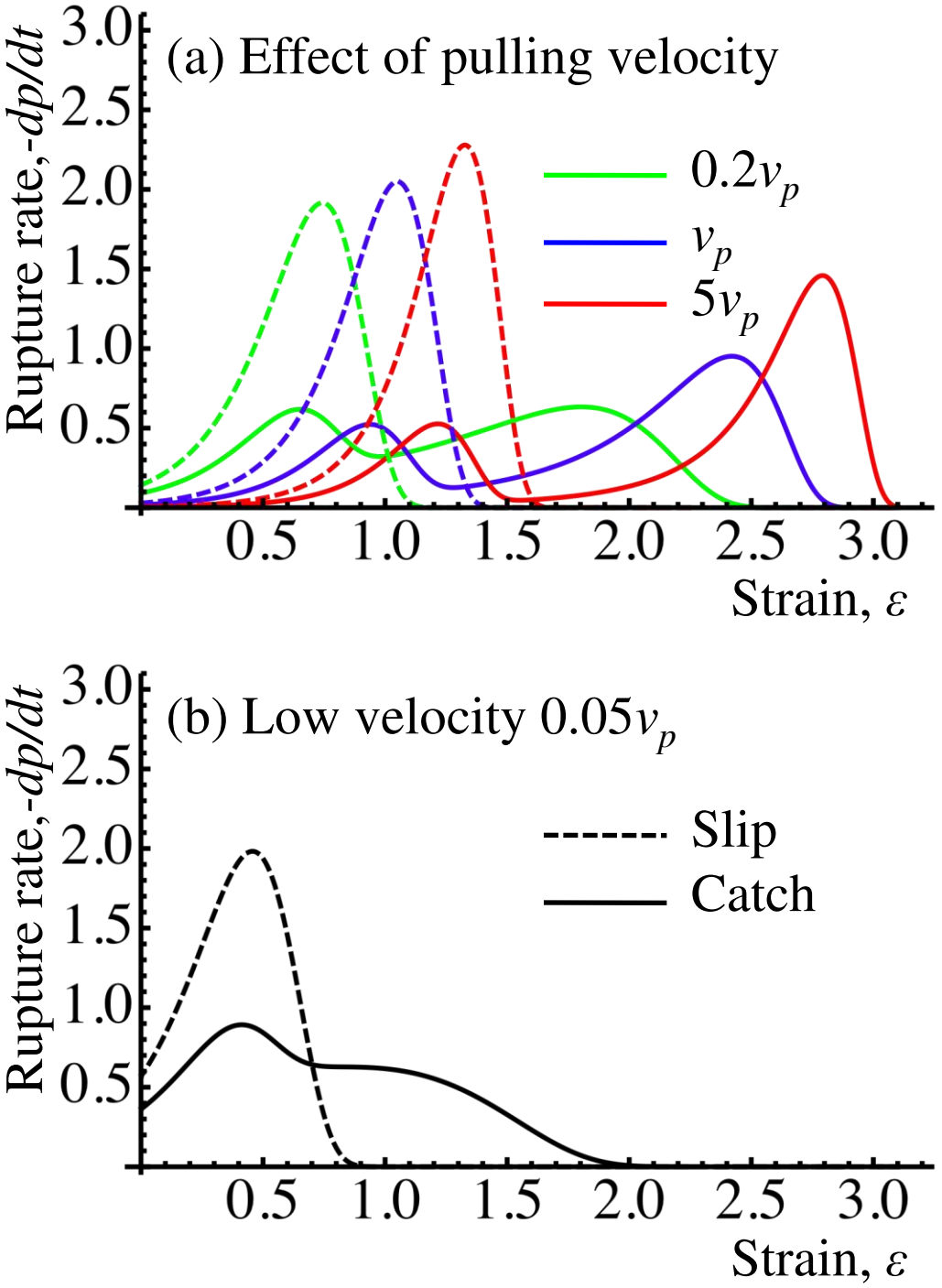
(a) Effect of pulling velocity
Rupture rate, -dp/dt
3.0
2.5
2.0
1.5
1.0
0.5
0.2v_p
v_p
5v_p
0.5
1.0
1.5
2.0
2.5
3.0
Strain, ε
(b) Low velocity 0.05v_p
Rupture rate, -dp/dt
Slip
Catch
Strain, ε

Fig. 3

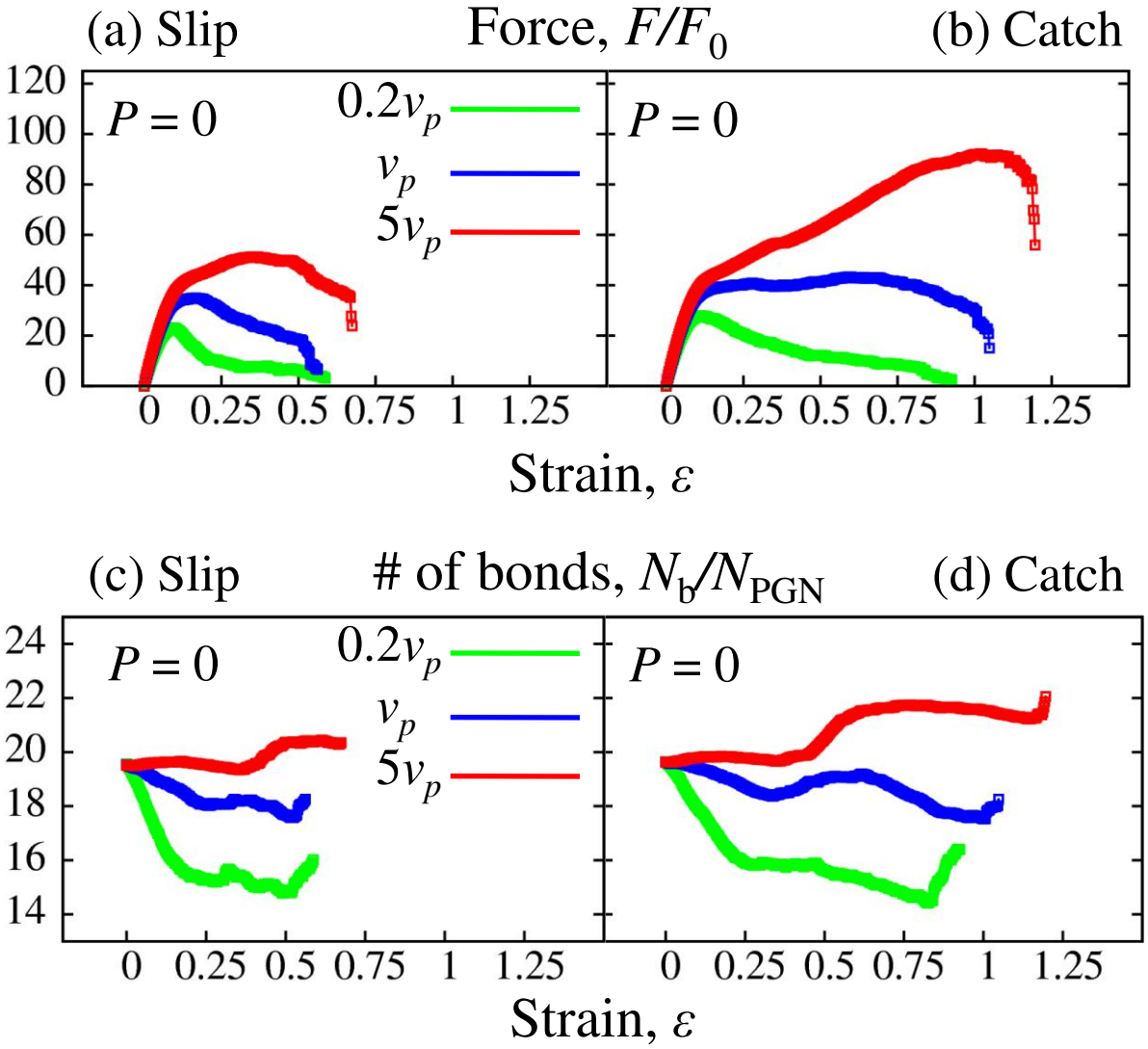
(a) Slip
Force, F/F_0
(b) Catch
$P = 0$
$0.2v_p$
v_p
$5v_p$
$P = 0$
120
100
80
60
40
20
0
0 0.25 0.5 0.75 1 1.25
0 0.25 0.5 0.75 1 1.25
Strain, ε
(c) Slip
# of bonds, N_b/N_{PGN}
(d) Catch
$P = 0$
$0.2v_p$
v_p
$5v_p$
$P = 0$
24
22
20
18
16
14
0 0.25 0.5 0.75 1 1.25
0 0.25 0.5 0.75 1 1.25
Strain, ε

Fig. 4

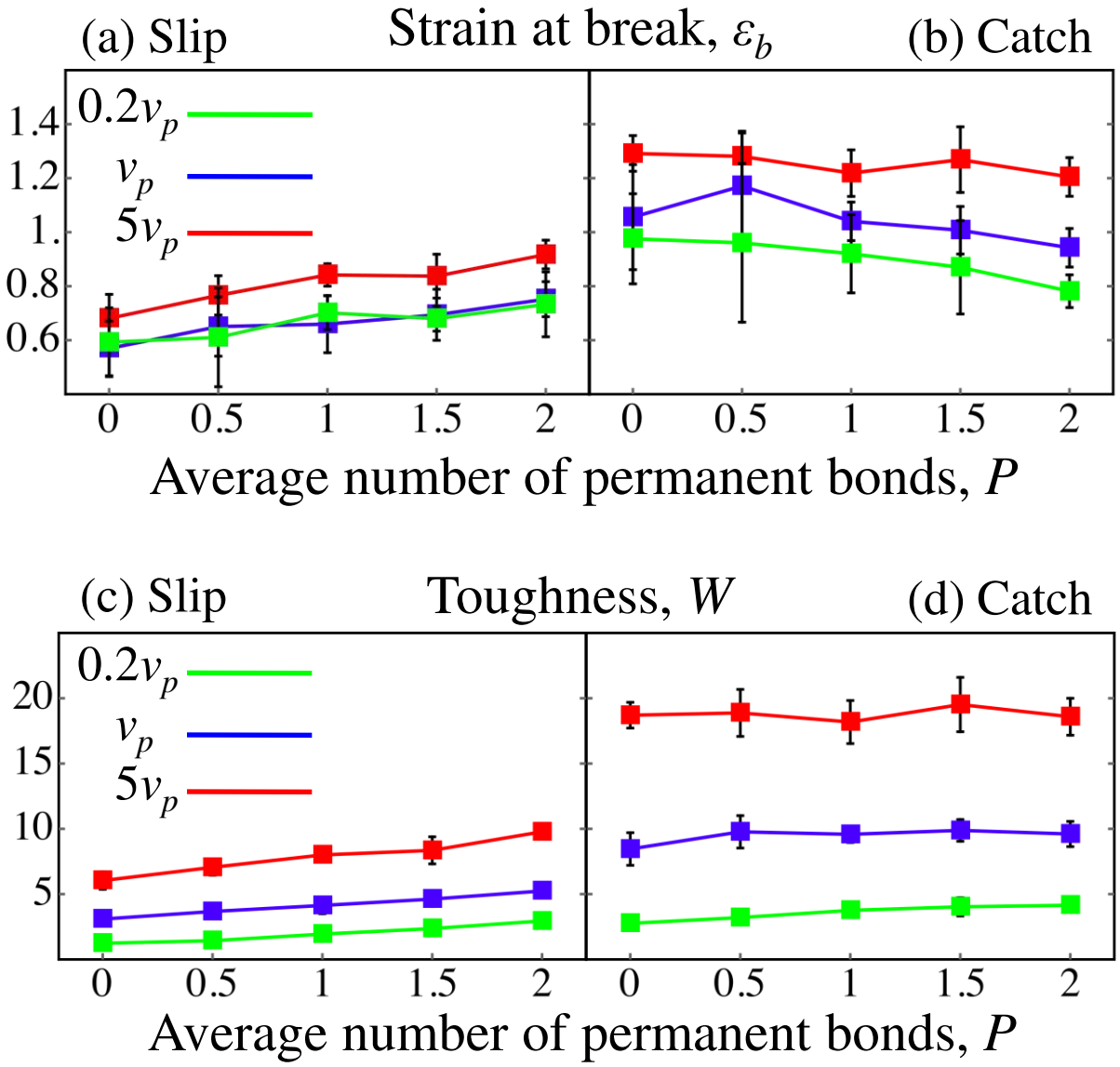
(a) Slip
Strain at break, ε_b
(b) Catch
$0.2v_p$
v_p
$5v_p$
1.4
1.2
1.
0.8
0.6
0
0.5
1
1.5
2
Average number of permanent bonds, P
(c) Slip
Toughness, W
(d) Catch
20
15
10
5
Average number of permanent bonds, P

Fig. 5

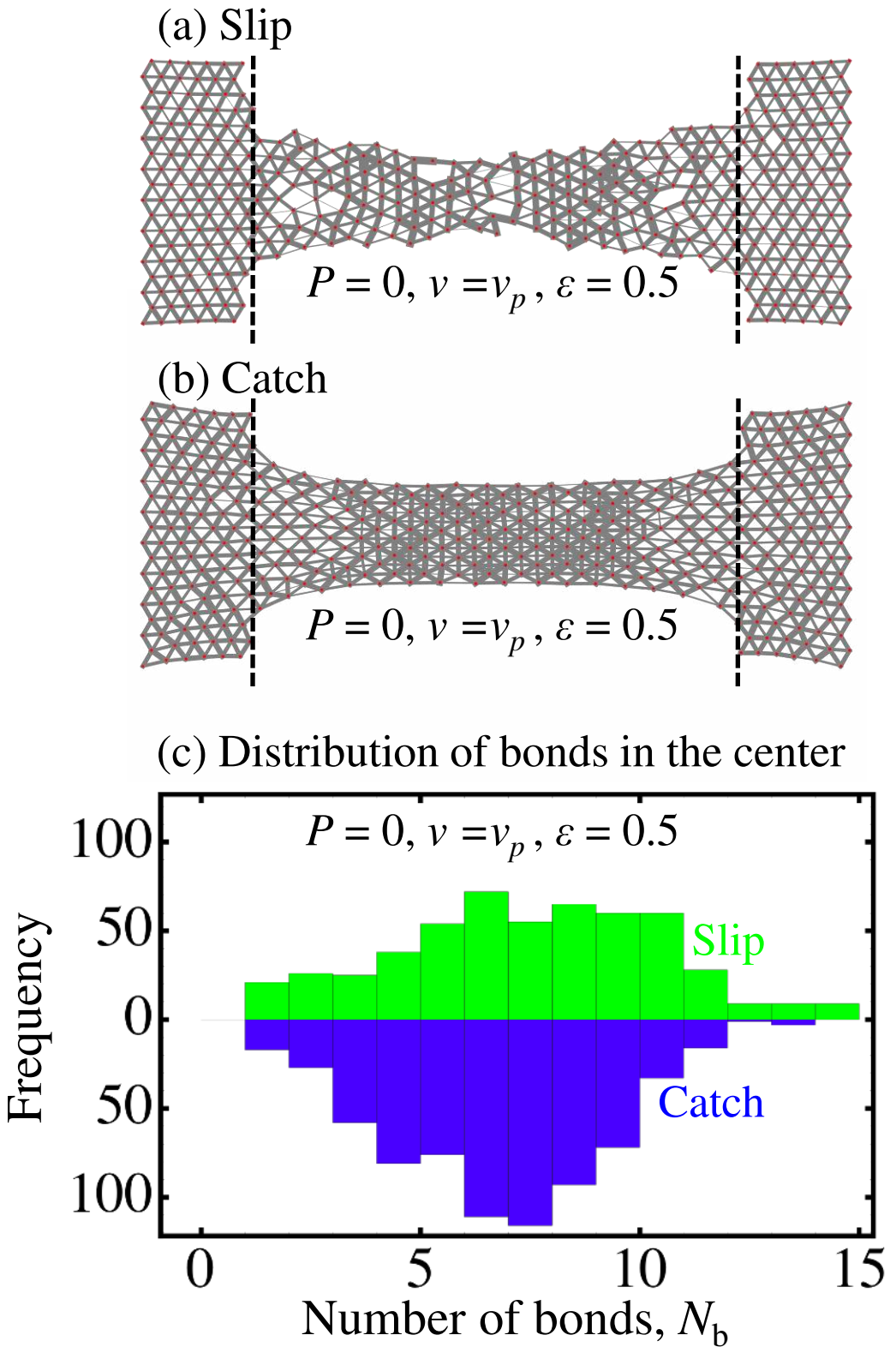
(a) Slip
$P = 0, v = v_p, \varepsilon = 0.5$
(b) Catch
$P = 0, v = v_p, \varepsilon = 0.5$
(c) Distribution of bonds in the center
$P = 0, v = v_p, \varepsilon = 0.5$
Slip
Catch
Frequency
100
50
0
50
100
0
5
10
15
Number of bonds, N_b

Fig. 6

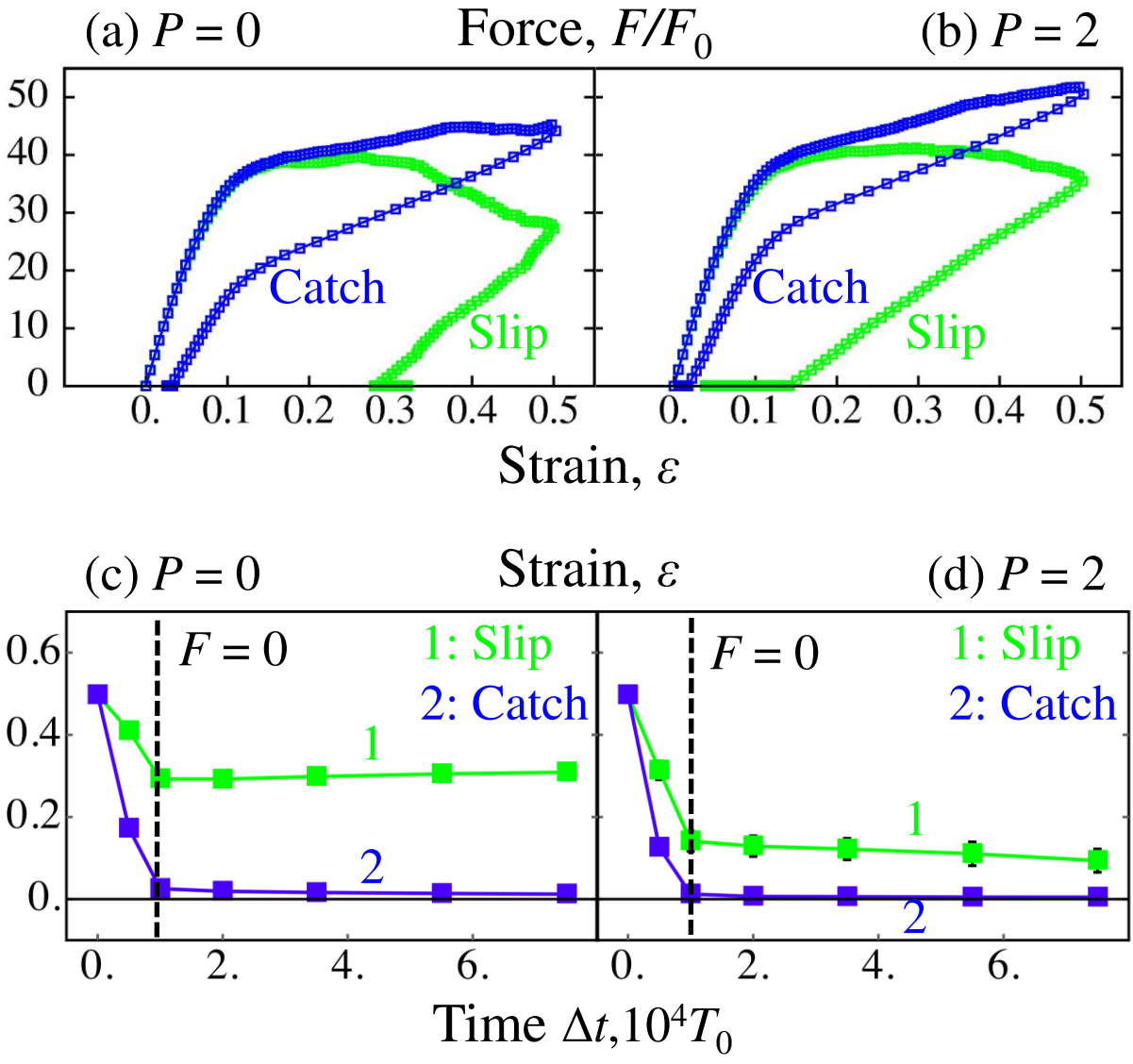
(a) $P = 0$
Force, F/F_0
(b) $P = 2$
50
40
30
20
10
0
Catch
Slip
Catch
Slip
0.
0.1
0.2
0.3
0.4
0.5
Strain, ε

(c) $P = 0$
Strain, ε
(d) $P = 2$
0.6
0.4
0.2
0.
$F = 0$
1: Slip
2: Catch
1
2
$F = 0$
1: Slip
2: Catch
1
2
0.
2.
4.
6.
Time $\Delta t, 10^4 T_0$

Fig. 7

(a) Multiple cycles at constant maximal strain

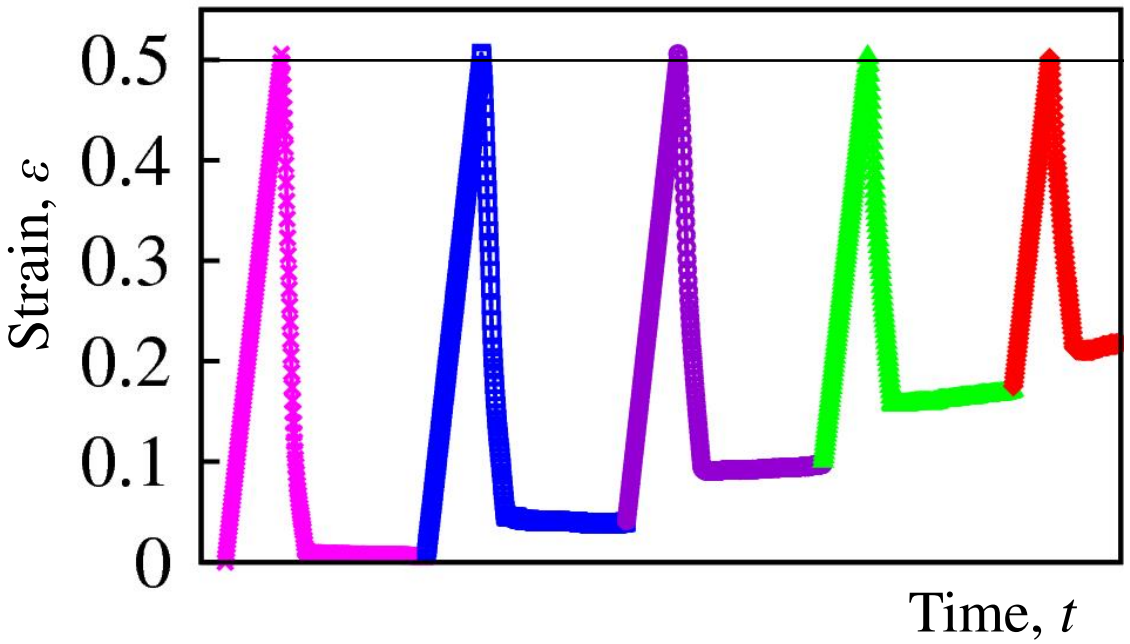

(b) Multiple cycles at increasing maximal strain

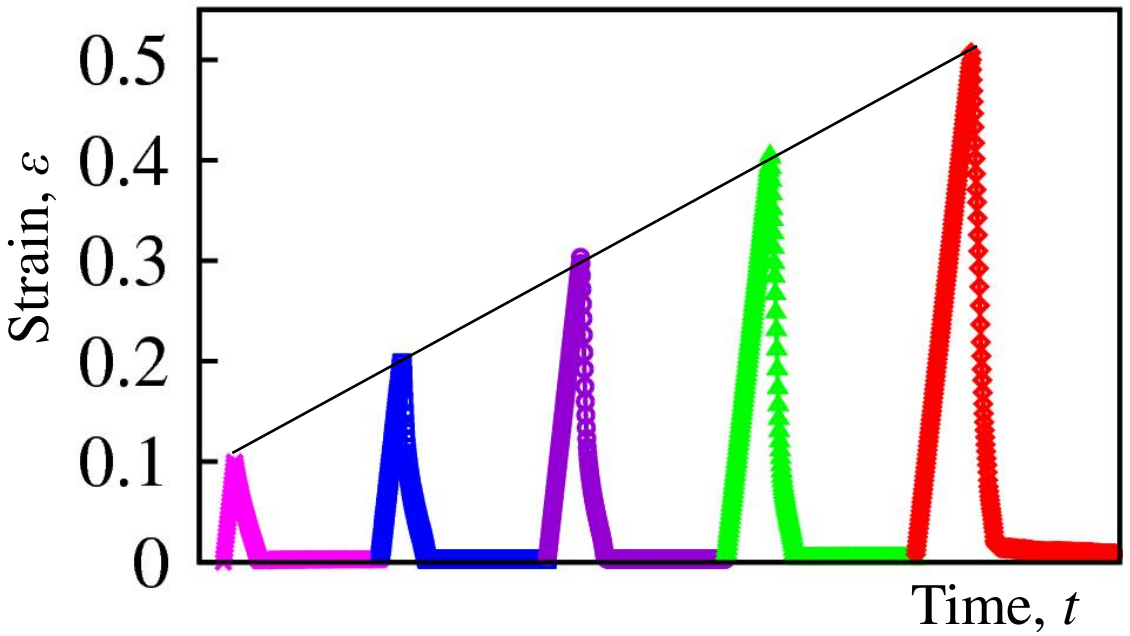

Fig. 8

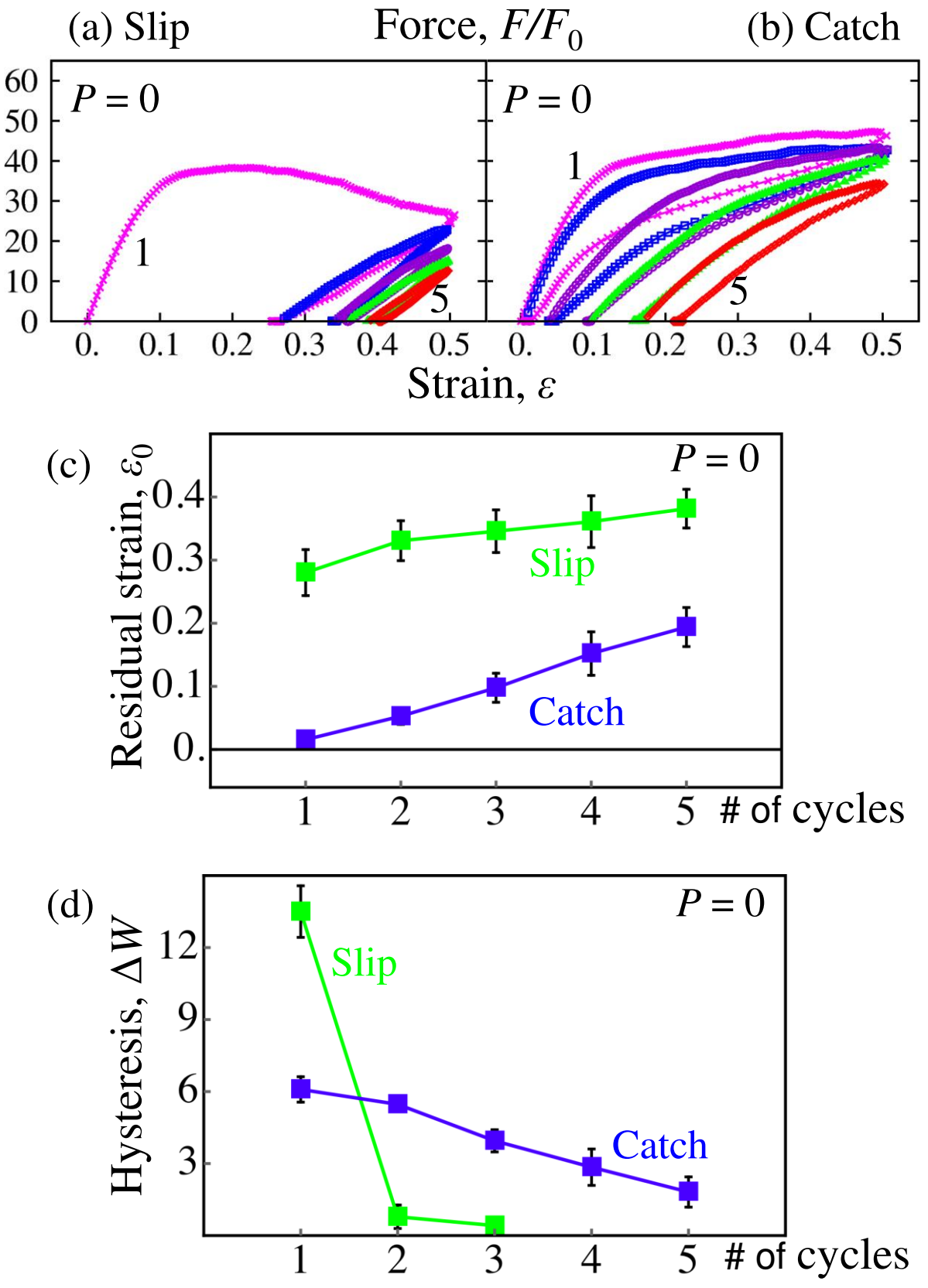
(a) Slip
Force, F/F_0
(b) Catch
$P = 0$
$P = 0$
1
5
1
5
60
50
40
30
20
10
0
0.
0.1
0.2
0.3
0.4
0.5
Strain, ε
(c)
Residual strain, ε_0
$P = 0$
Slip
Catch
0.4
0.3
0.2
0.1
0.
1
2
3
4
5
# of cycles
(d)
Hysteresis, ΔW
$P = 0$
Slip
Catch
12
9
6
3
1
2
3
4
5
# of cycles

Fig. 9

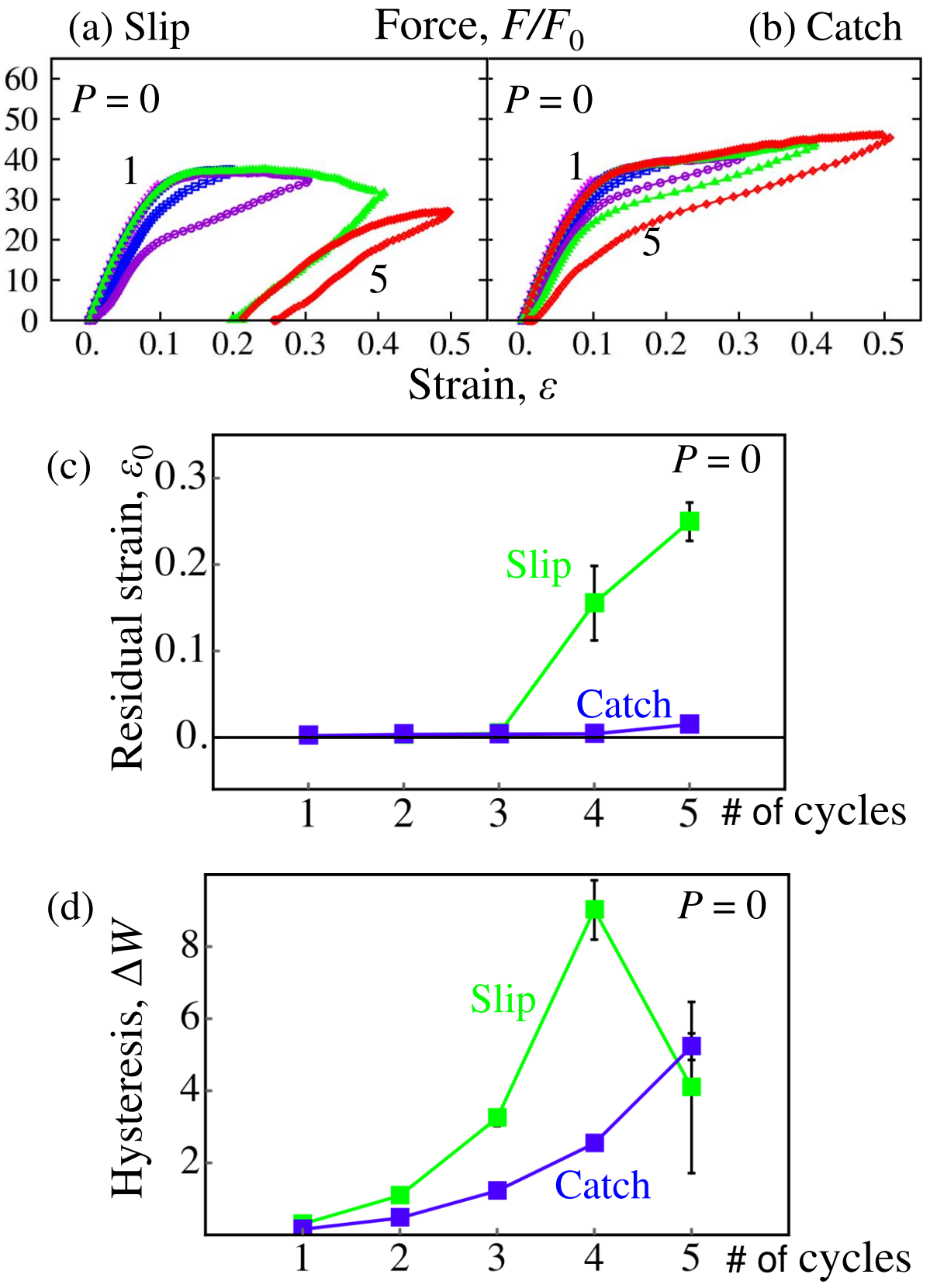
(a) Slip
Force, F/F_0
(b) Catch
$P = 0$
1
5
Strain, ε
(c)
Residual strain, ε_0
Slip
Catch
# of cycles
(d)
Hysteresis, ΔW
Slip
Catch
# of cycles

Fig. 10